Journal of
Applied Crystallography
ISSN 0021-8898

Received 21 December 2006
Accepted 24 January 2007

From CIF to virtual morphology using the *WinXMorph* program

Werner Kaminsky

Department of Chemistry, Seattle, Washington, USA. Correspondence e-mail: kaminsky@chem.washington.edu

Crystal morphologies are predicted from data stored in files in the CIF format (crystallographic information file standard of the International Union of Crystallography) on the basis of the Bravais–Friedel, Donnay–Harker model. Several simple improvements to the calculation are introduced with *WinXMorph*, version 1.4.9, in conjunction with illustrations of the morphologies of quartz, sucrose, lactose, pyrite and lysozyme. The morphologies of the recently discovered pentamorphs of 1,8-dihydroxyanthraquinone are predicted. *WinXMorph* is available free-of-charge for educational use.

1. Introduction

Who does not wonder what the crystals looked like from which X-ray structures have been reported? Abandoned is the tradition of illustrating morphology as in Groth's monumental compendium (Groth, 1906). The specific indices and sizes of observed crystal faces are no longer published, reducing the information to color, a rough size estimate, combined with teasing hints as to the habit ('plate', 'needle', 'prism' . . .), and surface characteristics ('dull', 'clear', 'metallic' . . .). Often crystals are disposed of after the structure has been determined. Optical goniometry is a lost art. For research related to growth of crystals and surface structure and reactivity, the lack of this information is regrettable. Moreover, the beauty of these crystalline forms is lost as well.

Here, I discuss how to recover lost morphologies from X-ray crystallographic data. The aesthetic aspects of crystals combined with virtual reality are contemporary ways of exciting a young student's interest in crystallography, as well as an aid in teaching the principles of crystal symmetry.

2. Symmetry independence of faces, polarity and lustre

From the beginnings of X-ray crystallography, researchers have attempted to predict crystal shapes [Bravais–Friedel, Donney–Harker model, BFDH model (Bravais, 1866; Friedel, 1907; Donnay & Harker, 1937)] from metric data, point-group symmetry and the systematic absences, all available in each of today's crystallographic information files written in the CIF format.

When real crystals grow, the shapes are far from the ideal morphologies created when applying the point-group symmetries to a 'unique' set of crystal faces. Despite this, a realistically predicted morphology needs to include the growth differences between symmetry-independent faces. There may be symmetry-distinct faces that are nevertheless predicted by the simplest BFDH implementation to have the same central distance because considerations based entirely on symmetry do not contain information about the molecular or atomic structure of these faces, which would be different if they were not related by symmetry, and thus, should grow at different speeds. A refinement of growth rate predictions is generally achieved with surface energy calculations [*e.g.* Hartman–Perdok model periodic bond chain analysis (Borm, 1923; Hartman & Perdok, 1955; Hartman, 1973), Ising model (Burton *et al.*, 1951; Jackson, 1958), attachment energy model (Berkovitch-Yellin, 1985), cellular automata (Wolfram, 2002), kinetic simulations (Rohl, 2003)]. Without this, the predicted morphology may not even be recognized as that of the specific crystal, even by the trained eye of a mineralogist, this despite the fact that no two crystals look the same.

To make matters worse, we cannot forget the influence of solvents on the crystal growth characteristics (Liu *et al.*, 1995; Benazet *et al.*, 2003). Are we then doomed to fail in our attempt to recover the crystal without a detailed treatment of the specific growth process?

I recently released a free-for-educational-use software package running under Microsoft Windows for drawing crystal shapes (Kaminsky, 2005) and have now implemented the BFDH model within that package, distributed under the name *WinXMorph*. Applying simple 'distortions' to a calculated morphology from the BFDH model, governed by refined symmetry considerations, helps to make predictions that are often closer to observed crystal habits than unmodified calculations and some intensive surface structure and interaction analysis calculations (of course, these calculations are of undisputed merit).

Quartz, space group $P3_12$ or $P3_22$, may serve as an example. The pyramidal {101} and {011} faces are not symmetry related. However, central distances calculated with BFDH from evaluating the length of face normal vectors, $|\mathbf{h}|$, $\mathbf{h}$ = (101) or (011), will be identical, obviously, as axes **a** and **b** are of equal length, although the surface structures are different. The differences introduced by evaluation of the structure and surface characteristics calculations are much smaller than those of the grown crystals, reaching roughly 1%, whereas the real quartz sample shows on average a difference of 10% in the central distances between (101) and (011), not to mention that the different morphology calculation models do not agree on which form will grow faster (Nicolov & Woensdregt, 2002).

One could, however, introduce arbitrary factors deviating to a certain percentage from unity to scale the faces within a set of 'unique' crystal faces to introduce the expected symmetry independency which will bring the predicted morphology closer to reality. A repetition of the calculations with a statistically applied scale to the forms will in addition give an overview of possible shapes one would observe in the field (Fig. 1).

If the symmetry belongs to a polar point group, I would like to suggest here that one could scale faces on opposite sides of a polar axis differently to simulate the expected growth rate variations:

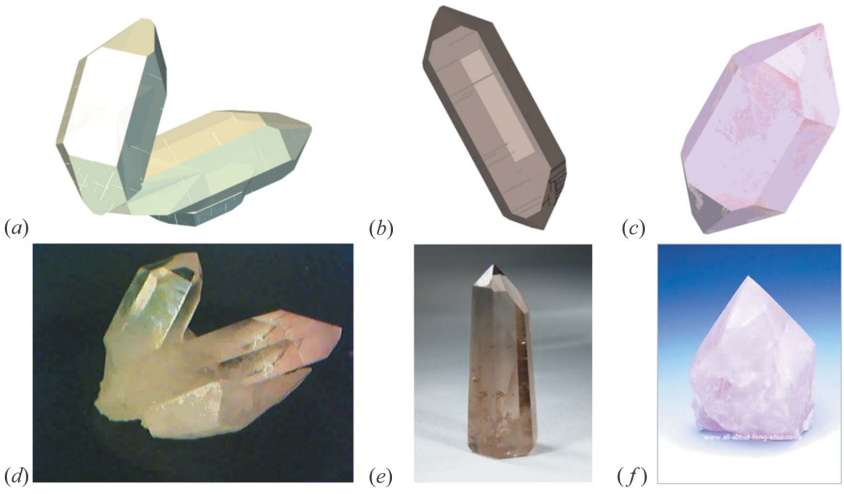

Figure 1
(*a*) Virtual quartz group. The shape was simulated with the modified BFDH model as well as rendered with *WinXMorph*, applying an up to 10% statistical scaling of independent faces, and standard textures (growth striations) of clear crystals were applied to the faces. Model crystals were then scaled and grouped. (*b*) Smoky quartz, with darker body, 20% variation between all faces. (*c*) Rose quartz with pink body and marbled surface. All models are freely moveable on the computer in real time. Real crystals: (*d*) author's photograph; (*e*) http://www.stonekeeper.com; (*f*) http://www.all-about-feng-shui.co.uk.

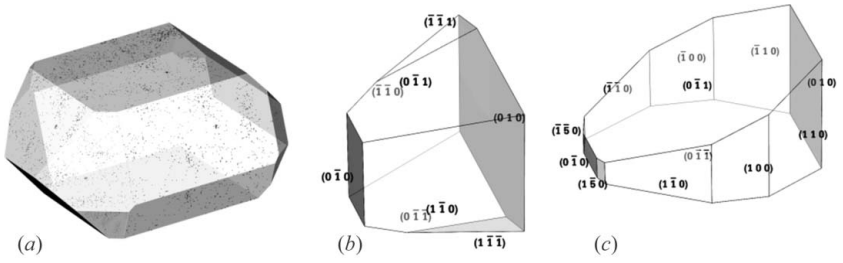

Figure 2
(*a*) Virtual sugar candy (sucrose), predicted with a standard 'dull surface' pattern and 50% polarity factor along the **b** axis. The shape is very close to the observed morphology for growth slightly above room temperature. (*b*) α-Lactose monohydrate calculated with 90% polarity, and restriction to Miller indices not larger than 1. (*c*) Typical morphology of α-lactose monohydrate.

(*a*)
```
_exptl_crystal_coloring_lustre  'dull'
loop_
 _exptl_crystal_face_index_h
 _exptl_crystal_face_index_k
 _exptl_crystal_face_index_l
 _exptl_crystal_face_perp_dist
   -1  -1  0     0.725
   -1  -1  1     0.764
   -1   0  0     0.548
   -1   0  1     0.597
    0  -1  -1    0.616
    0   0  -1    0.391
    0   1  -1    1.355
```

(*b*)

Figure 3
(*a*) CIF syntax for lustre, faces, and central distances for the sugar model in Fig. 2. (*b*) 'Dull' lustre.

$$D_x = D_{x-\text{calculated}}\left[1 - p\,\text{sgn}(h_x)\,h_i \Big/ \left(\sum_j h_j^2\right)^{1/2}\right]. \qquad (1)$$

D_x is the central distance of face h, h_i are the Miller indices and p is the polarity, taking values between 0 and 1. Faces at larger angles towards the polar direction parallel to $h_x\mathbf{a}_x^*$ should be less affected by the polarity. This is introduced by the geometric weight (square root of the sum of squared indices).

Sucrose (Wang *et al.*, 2000) and α-lactose monohydrate (Clydesdale *et al.*, 1997) (Fig. 2) are good examples of the improved realism obtained this way.

The CIF format allows reports of hydrogen bonds, which are known to have a pronounced impact on the morphology (Docherty *et al.*, 1991). Along such bonds, growth rates are higher and a further refinement of the morphology is at hand when inspecting the reported bonds, provided they have been added to the CIF file.

Once a morphology has been created, the Miller indices and central distances should be saved. The International Union of Crystallography (IUCr) has devised a syntax (rarely used in the past) that allows the addition of this information and the surface properties to the CIF file. An example of such a listing is given for sugar (Fig. 3).

At the end of the day, however, real crystal faces are scratched or etched *etc*., and reflect as well as refract light in characteristic ways. The *WinXMorph* program accommodates transparency and texture. In this way one can 'handcraft' museum-quality virtual crystals on the computer (Figs. 4 and 5).

3. Application to polymorphism

3.1. Lysozyme

A thorough morphology study of hen egg-white lysozyme was published by Matsuura & Chernov (2003) in which 'the strengths of intermolecular contacts (macro bonds) and the areas occupied by each contact on the molecular surface were estimated in four polymorphic modifications of lysozyme crystals based on the bond strengths between individual atomic pairs belonging to the molecules in contact' (Fig. 6).

In a protein crystal, polarity may not be that important. Thus, the calculations were carried out with only up to 10% polarity for the monoclinic form. A perfect match of the BFDH model is observed for the tetragonal morphology. The orthorhombic crystals do not show the estimated {101} face, which is the fastest growing in the BFDH model.

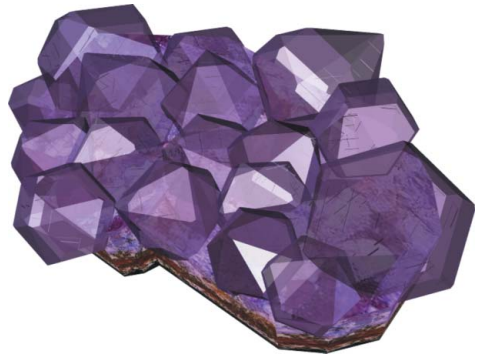

Figure 4
Virtual amethyst aggregate created from a *WinXMorph* model assembled on a substrate model using VRLM commands. This image can be rotated in real time on the computer screen.

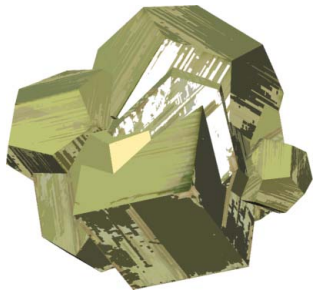

Figure 5
Virtual pyrite hand piece created from *WinXMorph* models and grouped using VRLM commands. This image can be rotated in real time and in any direction on the computer screen.

Crystal data	1	2	3	4
Formula	$C_{14}H_8O_4$	$C_{14}H_8O_4$	$C_{14}H_8O_4$	$C_{14}H_8O_4$
Color, habit, lustre	colorless **prism** clear	colorless **prism** clear	colorless **prism** clear	colorless **prism** clear
Crystal system	Tetragonal	Orthorhombic	Monoclinic	Triclinic
Space group	$P4_12_12$	$P2_12_12_1$	$P2_1$	$P\bar{1}$(#2)
a, Å	78.54	56.44	26.90	27.28
b, Å	78.54	73.73	58.95	31.98
c, Å	37.77	30.43	31.33	34.29
α, °	90	90	90	88.53
β, °	90	90	111.9	108.57
γ, °	90	90	90	111.85
Observed	{101}, {110}	{010}, {011}, {110}	{100}, {001}, {10-1}, {010}	N/A
Calculated Matsuura et al., 2003	{101}, {110}, {100}, {001}	{010}, {011}, {110}, {100}, {001}, {101}	{100}, {001}, {10-1}, {010}, {101}, {110}, {011}	N/A
Extrapolated Morphology (BFDH-model)	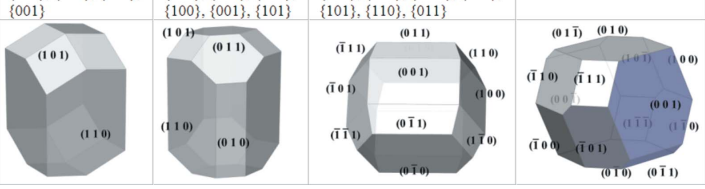			

Figure 6
Polymorphs of lysozyme (Matsuura & Chernov, 2003) and morphology calculations.

Crystal data	1	5	2	3	4
Formula	$C_{14}H_8O_4$	$C_{14}H_8O_4$	$C_{14}H_8O_4$	$C_{14}H_8O_4$	$C_{14}H_8O_4$
Color, habit, lustre	orange, **plate** (fragment) clear	red-orange, **'block'** clear	orange, **needle** (fragment), clear	orange, **prism** clear	orange, **needle** (fragment) clear
Sample size (mm)	0.22x0.12x0.07	0.37x0.34x0.28	0.24x0.07x0.05	0.43x0.43x0.12	0.26x0.09x0.08
Crystal system	Tetragonal	Tetragonal	Orthorhombic	Triclinic	Monoclinic
Temperature	130(2)	295(2)	130(2)	130(2)	110(2)
Space group	$P4_1$ (#76)	$P4_12_12$ (# 92)	$Pca2_1$ (#29)	$P\bar{1}$(#2)	$P2_1/n$ (#14)
a, Å	5.7230(3)	5.7440(6)	21.578(2)	10.2110(15)	7.2930(5)
b, Å	5.7230(3)	5.7440(6)	3.7660(16)	10.3080(15)	9.5001(7)
c, Å	30.923(2)	31.393(3)	24.683(2)	19.776(3)	14.7208(11)
α, °	90	90	90	78.058(8)	90
β, °	90	90	90	83.905(9)	91.634(2)
γ, °	90	90	90	88.995(11)	90
Directional hydrogen bonds	ca. along <100>	ca. along <100>	unspecific	unspecific	unspecific
Observed faces	(001), (00$\bar{1}$), (10±1)	{001}, {101}		{100}, {010}, {001}	N/A
Extrapolated morphology	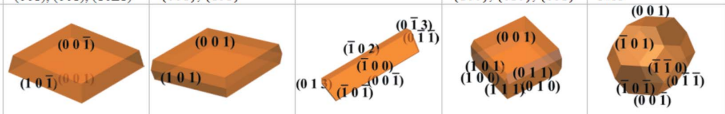				
Birefringence, Δn micrographs & eigenmodes of slow axis (white lines)	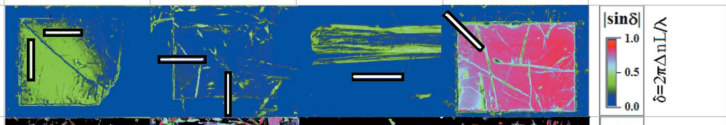				
Extinction angle micrographs of eigenmodes of slow axis					

Figure 7
Morphological details of the known polymorphs in 1,8-dihydroxyanthraquinone. The optical micrographs of the birefringence help to differentiate between the polymorphs. Polymorph 1, calculated with 20% polarity, is known to show strong anomalous birefringence in contrast to 5, which is almost perfectly extinct along the optic axis with a small reminiscence of {101} growth sectors. Polymorph 3 exhibits extinction at an angle close to 135° and the intrinsic birefringence is fairly strong. When looking along (001), the crystals are pseudo orthogonal at an angle of $\gamma = 88.995\ (11)^\circ$. No micrograph was available for polymorph 4. All samples were *ca* 1 mm across. Because of strong linear dichroism, the extinction angle shown for polymorph 2 appears 45° clockwise rotated. The phase factor $\delta = 2\pi\Delta nL/\lambda$ is related to the birefringence, Δn, wavelength of light, λ, and sample thickness, L. Further details of polarimetric methods used here are outlined elsewhere (Kaminsky *et al.*, 2004).

The estimates for the monoclinic case include the observed faces, but also several additional faces. Including a polarity factor did not improve the estimate.

There are no indexing data for the triclinic crystal faces available. The estimated morphology will give a first impression of what the crystals might have looked like of which the structure was determined.

3.2. 1,8-Dihydroxyanthraquinone

1,8-Dihydroxyanthraquinone (DHA) crystallizes under different conditions in five different polymorphs (Fig. 7) (Claborn *et al.*, 2007; Zain & Ng, 2005). The tetragonal (polymorphs 1 and 5) and orthorhombic (2) modifications were indexed *via* X-ray diffraction on a Nonius–Bruker KAPPA CCD X-ray diffractometer (Mo $K\alpha$ radiation).

Polymorph 1 was grown from the slow evaporation of a 50:50 (*v*/*v*) acetone/acetonitrile solution of 1,8-dihydroxyanthraquinone (Aldrich) over the course of 2–3 days to a size of 0.5 cm × 0.5 cm × 100 µm. The crystals were often raised in the center and along the borders between lateral growth sectors. Needles of polymorph 2, typically 500 µm long and 10–70 µm wide, were formed in the same way as 1 but with faster evaporation rates (~24 h). On average, in the growth experiments of polymorph 1, one in a hundred of the prismatic plates belonged to polymorph 3. Form 4 was obtained by sublimation at 393–398 K under vacuum (3–5 torr). Form 5 was grown by evaporation from pyridine. Forms 1, 2, 4, and 5 melt at 467–469 K and 5 transforms under cooling into 1, exhibiting a domain structure related by a twofold rotation along [110].

Polymorphs 1 and 5 are of special interest as both crystallize as wafer-thin plates with {001} faces of several millimetres across, to which the extinction condition of a 4_1 screw axis would have to be applied, which causes an increased prismatic appearance. The growth of polymorph 5 is slightly more prismatic than 1, although structurally very closely related to 1, with an additional 2_1 screw axis along ⟨100⟩.

When trying to calculate the morphology for 1 and 5 without further modifications, one would obtain a compact prism similar to 3, which is not observed in either of these polymorphs

Additional inspection of the structure is required. From a packing diagram of the structure or a table of hydrogen bonds, one sees intermolecular hydrogen bonds between the ketone and one hydroxyl group along *ca* ⟨100⟩, and strong dipolar coupling forces along ⟨110⟩ in each of the four levels per unit cell perpendicular to the 4_1 screw (Claborn *et al.*, 2003). Only weak van der Waals forces connect the molecules along the **c** axis. The projection of the net-dipole onto the **c** axis is negligible. The strong dipoles will promote growth of the {110} faces. The directional hydrogen bonds will promote growth of the {100} faces (Fig. 8).

We may expect that the four hydrogen bonds and dipoles per unit cell in polymorphs 1 and 5 effectively outbalance the 4_1 screw-axis restriction to

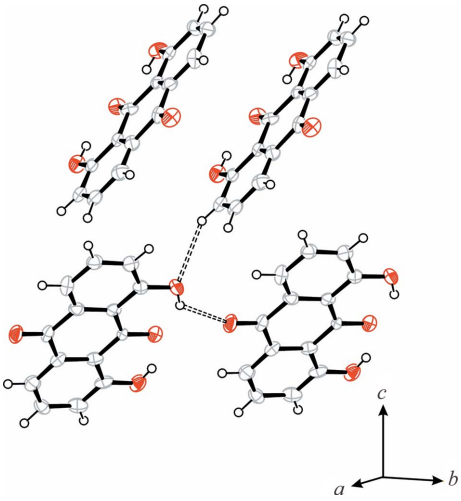

Figure 8
Packing diagram of DHA, polymorph 1. Along *ca* ⟨100⟩ are found hydrogen bonds between the hydroxyl and ketone. A permanent dipole points along *ca* ⟨110⟩. Weak van der Waals forces along **c** are indicated by the dotted line between the hydroxyl and aromatic hydrogen.

(001) and (0$\bar{1}$1) faces. The thin shapes calculated for polymorphs 1 and 5 in the case that the 4_1 screw was completely neglected are much closer to the observed morphology. The 2_1 screw axis in 5 has the additional effect on the morphology of eliminate the {100} faces. Because of the strong structural correlation between 5 and 1, it could be speculated that polymorph 1 possesses a pseudo 2_1 axis that would in addition elongate growth along ⟨100⟩. This may explain why {100} faces are not observed in 1 as well as 5.

Of polymorph 2, it is only known that the **b** axis is along the needle elongation, which is confirmed in the BFDH calculations. Crystals of 3 were similar to 1 but thicker, which the BFDH model confirms. The prismatic character of 4 does not match the reported crystal size; here the predicted shape is unlikely.

Polar factors of up to 20% were allowed in the *WinXMorph* calculations for polymorph 1, which eliminated one set of {101} faces, but similar large statistical variances were found to have little effect in the other polymorphs.

4. Summary

WinXMorph allows a 'best guess' recovery of the crystal habit of an incompletely edited CIF file, provided that hydrogen bonds and possible dipoles are analyzed for a further refinement of the model. The ability to introduce statistical or polar variances and face lustre results in realistic virtual crystal models.

I am grateful for support by the National Science Foundation (CHE-0092617). Thanks are also owed to Bart Kahr for providing the polymorph 5, to Kacey Claborn for the second polymorph 2 of 1,8-dihydroxyanthraquinone, and to Massimo Moret for providing information on polymorph 4.

References

Benazet, S., Jacob, G. & Pepe, G. (2003). *Propellants Explosives Pyrotechnics*, **28**, 287–295.
Berkovitch-Yellin, Z. (1985). *J. Am. Chem. Soc.* **107**, 8239–8253.
Borm, M. (1923). *Atom Theorie des festen Zustandes*, 2nd ed., p. 538. Leipzig: Engelmann.
Bravais, A. (1866). *Du Cristal Considere Comme un Simple Assemblage de Points, Etude Cristallographiques*. Paris: Gauthier-Villars.
Burton, W. K., Cabrera, N. & Frank, F. C. (1951). *Philos. Trans. R. Soc.* **243**, 299–358.
Claborn, K., Kaminsky, W., Kahr, B., Moret, M. & Rohl, A. L. (2007). *Cryst. Growth. Res.* Submitted.
Claborn, K., Puklin-Faucher, E., Kurimoto, M., Kaminsky, W. & Kahr, B. (2003). *J. Am. Chem. Soc.* **125**, 14825–14831.
Clydesdale, G., Roberts, K. J., Telfer, G. B. & Grant, D. J. W. (1997). *J. Pharm. Sci.* **86**, 135–141.
Docherty, R., Clydesdale, G., Roberts, K. J. & Bennema, P. (1991). *J. Phys. D. Appl. Phys.* **24**, 89–99.
Donnay, J. D. H. & Harker, D. (1937). *Am. Mineral.*, **22**, 446–467.
Friedel, G. (1907). *Bull. Soc. Fr. Mineral.* **22**, 326–455.
Groth, P. (1906). *Chemische Kristallographie*. Leipzig: Engelmann.
Hartman, P. (1973). *Crystal growth: An Introduction*, p. 367. Amsterdam: North-Holland.
Hartman, P. & Perdok, W. G. (1955). *Acta Cryst.* **8**, 49–52.
Jackson, K. A. (1958). *Liquid Metals and Solidification*, p. 174. Cleveland: American Society of Metals.
Kaminsky, W., Claborn, K. & Kahr, B. (2004). *Chem. Rev. Soc.* **33**, 514–525.
Kaminsky, W. (2005). *J. Appl. Cryst.* **38**, 566–567.
Liu, X. Y., Boek, E. S., Briels, W. J. & Bennema, P. (1995). *Nature (London)*, **375**, 342–345.
Matsuura, Y. & Chernov, A. A. (2003). *Acta Cryst.* D**59**, 1347–1356.
Nicolov, M. F. & Woensdregt, C. F. (2002). *J. Appl. Cryst.* **35**, 491–496.
Rohl, A. L. (2003). *Curr. Opin. Solid State Mater. Sci.* **7**, 21–26.
Wang, B., Silber, C. & Follner, H. (2000). *Chin. Sci. Bull.* **45**, 1468–1471.
Wolfram, S. (2002). *A New Kind of Sciences*. Champaign: Wolfram Media.
Zain, S. M. & Ng, S. W. (2005). *Acta Cryst.* E**61** o2921–o2923.